Published in the International Journal of Adhesion and Adhesives
DOI: https://doi.org/10.1016/j.ijadhadh.2020.102691

Effect of Elevated Temperatures and Humidity on Glass/Steel Adhesive Joints

Ioannis Katsivalis[a] , Ole Thybo Thomsen[b], Stefanie Feih[c*] and Mithila Achintha[d],

[a] Department of Engineering, University of Cambridge, Trumpington Street, CB2 1PZ, UK

[b] Bristol Composites Institute, Department of Aerospace Engineering, University of Bristol, Bristol BS8 1TR, UK

[c] Polymer Processing Group, Singapore Institute of Manufacturing Technology (SIMTech), 73 Nanyang Drive, Singapore 637662

[d] Faculty of Engineering and Physical Sciences, University of Southampton, Southampton SO17 1BJ, UK

Keywords: B. Glass, C. Finite Element Analysis, D. Cohesive zone model, D. Durability, Environmental exposure, Humidity, Elevated temperature

Glass/steel adhesive joints are being used increasingly in the construction industry as they offer significant structural advantages. While humidity and elevated temperatures are known to lead to the degradation of both the bulk adhesive materials and the bonded interfaces, quantification and prediction of the degradation effects are currently lacking. In this paper, the effects of elevated temperatures and humidity were determined and predicted by employing a combined experimental and numerical methodology. Bulk material and interface characterisation tests were performed to quantify the degradation of the bulk material properties and the glass/steel interfaces. Two numerical methodologies were devised and compared based on their ability to predict failure of glass/steel adhesive joints following environmental exposure, namely a continuum mechanics approach based on the bulk properties of the adhesive, and a cohesive zone modelling approach that assesses damage and failure based on the glass/steel interface properties. The results highlight the significantly different relative contributions of bulk property and interface degradation depending on the type of adhesive used.

1. Introduction

The use of glass has increased significantly in the construction industry sector over the past few decades motivated by emerging architectural trends. However, the relatively low strength combined with the brittle nature of the material makes stress concentrations particularly undesirable for any glass structure [1]. Stresses accumulate in load introduction and connection points [2]. For assembly purposes, mechanical fasteners are used extensively in glass structures, but they a) lack structural efficiency since drilling is required which leads to surface flaws, b) introduce local stress concentrations due to undesirable contacts, and c) introduce an added mass/weight penalty to the structure.

* Corresponding author
Email addresses: ik384@cam.ac.uk (I. Katsivalis), o.thomsen@bristol.ac.uk (O.T. Thomsen), feihs@simtech.a-star.edu.sg (S. Feih), Mithila.Achintha@soton.ac.uk (M. Achintha)

According to IStructE [3], the use of adhesive joints in glass buildings have structural advantages compared to mechanical fasteners as they distribute the stresses more evenly over the area of the joint, do not increase the overall weight and also have perceived aesthetic advantages. However, adhesive joints are sensitive to environmental exposure. According to Van Lancker et al. [4], a lifetime of 20 to 25 years is expected for connections in building facades, but factors like temperature variation and high humidity can significantly reduce this time. The effect of high and low temperatures and humidity on the interfaces of adhesive joints remain topics of high research priority. Also, the effect of environmental exposure of adhesive joints manufactured using dissimilar substrates, for example, glass/metal adherends, may differ on each side of the joint due to dissimilar surface chemistry of the adherends.

The performance of glass adhesive joints subjected to environmental conditioning such as high/low temperatures, humidity and ultraviolet radiation has been studied by several research groups. An exposure cycle including moisture, high/low temperature and ultraviolet radiation was developed by Van Lancker et al. [4] to evaluate the performance of glass/steel adhesive connections. Different environmental conditions were studied both together and separately in an attempt to uncouple their respective contributions to the degradation of the joints.

A laboratory ageing cycle for glass adhesive joints was developed by Machalicka and Eliasova [5]. The cycle intended to simulate five years of outdoor exposure representing the climate of the Czech Republic by including moisture, high/low temperature variations and ultraviolet radiation exposure. Adhesives with different mechanical properties were included in this study, and they displayed different responses and effects upon environmental exposure. It was highlighted by the authors that the relationship between the environmental degradation of the adhesives and time is highly non-linear, and it is therefore very difficult to make accurate predictions regarding the performance of adhesive joints at different times.

ETAG 002 [6] is a European guideline relating to the use of structural sealants for facades introducing guidelines for material degradation for the use of bonded assemblies in the glass construction industry. ETAG 002 focuses on the use of structural sealants, mainly silicones, and stiffer adhesives such as epoxy resins and acrylates are not covered by the directive. The environmental cycle proposed by ETAG 002 introduces both humidity and elevated temperatures and can therefore be used as a reference to study the effect of these parameters on glass/steel adhesive joints. This was done in [7, 8] which used the proposed environmental cycle to evaluate adhesive joints for façade applications with metallic substrates. However, the interface response of hybrid glass/steel joints was not considered.

Several studies have tried to explain the underlying degradation mechanisms in the adhesive and the physical factors controlling these changes. For instance, Brewis et al. [9] studied the effect of moisture and elevated temperature on single lap joints and attributed the strength degradation to adhesive plasticization. Costa et al. [10] and Viana et al. [11] studied the effect of humidity on the performance of double cantilever beam specimens and observed swelling and possibly hydrolysis leading to chemical degradation of the adhesives used. In addition, Viana et al. [11] also determined that a fast diffusion path existed along the substrate/adhesive interface accelerating the joint degradation.

Our literature review shows that many studies are focusing on the experimental analysis of adhesive joints exposed to specific environmental conditions. This type of work is crucial in order to identify and certify suitable adhesives for the building industry, especially when joining different types of materials. However, the detailed experimental testing regime is cumbersome and expensive. Finite Element (FE) methods can be used as a predictive tool since the environmental exposure and the subsequent effects on the joints can be simulated. However, a validated predictive approach for the strength analysis and failure prediction of glass adhesive interfaces subjected to environmental exposure is still missing. Several studies focusing on non-glass substrates have adopted FE based analysis tools to simulate the degrading effect of environmental exposure in adhesive connections, either by considering the degradation of the bulk properties of the adhesive (assuming cohesive damage such as in Sugiman et al. [12]), or by considering the interface degradation (assuming adhesive damage such as in Liljedahl et al. [13]). However, it remains unclear how these two numerical approaches compare, and consequently which approach should be chosen in the case of glass-to-steel adhesive joining.

To fill this research gap, a detailed experimental test program on glass/steel joints before and after environmental exposure was conducted. The guidelines of ETAG 002 for defining suitable environmental cycles were followed. Both adhesive bulk property degradation and interface degradation of glass/steel joints were determined to derive the relevant input parameters for numerical modelling methodologies based on a Continuum Mechanics (CM) and a Cohesive Zone Modelling (CZM) approach. The numerical outcomes are compared to determine the model's ability to predict the mechanical property reduction of large double lap adhesive joints under four different load cases [14, 15] when exposed to simultaneous conditions of elevated temperatures and humidity. This approach also allows for direct identification of the dominant failure mechanism driving strength degradation in the case of competing adhesive and interface degradation effects.

2. Methodology

2.1 Adhesive characteristics and curing conditions

Two adhesives with significantly different behaviour were investigated in this study. The first adhesive, Araldite 2020 (Huntsman) is a brittle 2-part, clear, epoxy resin, and the second adhesive, Araldite 2047-1 (Huntsman), is a ductile 2-part methacrylate. The terms “brittle” and “ductile” are used in this work to differentiate the two adhesives based on their mechanical characteristics and their respective ability to deform under loading. The adhesives were cured for one week at ambient conditions as per manufacturers’ recommendations before environmental exposure. According to the manufacturers’ datasheets, the glass transition temperature (T_g) of the epoxy resin is 40 °C, while for the methacrylate it is 80 °C under these curing conditions.

2.2 Substrate characteristics

All specimens used in this study consisted of mild steel and tempered glass. Float tempered glass was used according to the specifications provided in BS EN 572-2:2012 [16] and BS EN 12150-1:2015+A1:2019 [17]. The mild steel was a low carbon grade supplied as hot rolled (S275R). The stresses developed in the steel substrates were significantly lower than the yield stress of the S275R mild steel and failure subsequently always initiated on the glass side.

2.3 Environmental conditioning

The guidelines of ETAG 002 [6] were followed for the environmental conditioning of adhesive joints followed in this study. More specifically, the exposure conditions considered were a full immersion in demineralised water for a duration of 3 weeks at a temperature of 45 °C. It should be noted that according to the guidelines the test specimens were positioned at least 20 mm below the water level and the temperature was monitored at frequent intervals and controlled by a universal oven. Following, the test specimens were removed from the oven and tested after conditioning at (23 ± 3) °C and (50 ± 5)% R.H. for (24 ± 4) hours. The ETAG guideline suggests that ultraviolet exposure should also be considered for glass adhesive joints. The focus of this work, however, was limited to studying the effect of hygrothermal exposure, and as a result ultraviolet exposure was not considered.

The selected temperature for the environmental exposure study corresponds to operational conditions in glass structures and therefore has practical relevance. Higher temperatures were considered during initial preliminary studies (60 °C and 80 °C), but both exposure temperatures led to full delamination

of the joints after a few days of exposure. These results were therefore not applicable to the present numerical study and are not included in this study.

It is worth noting that a coating (Hi-Pon 50-01 Polyurethane Top Coat) was used for the steel substrates during environmental exposure. This was to prevent excessive corrosion debris in the exposure tank leading to a change in the exposure water consistency and to thus minimize variability in the exposure conditions. The paint was applied after the glass/steel bonding was completed and therefore was assumed to have a negligible effect on the bonding quality. Furthermore, the coating was not applied to the sides of the bonded areas and therefore did not seal the joint to allow uninterrupted water diffusion.

2.4 Experimental methodology

Three different sets of tests were conducted. The first set of tests was conducted on tensile dogbone specimens (see Fig. 1a) and was used to evaluate the mechanical property degradation of the two adhesives considered in this study. The tests were conducted as per ISO 527-1:2012 and 527-2:2012 standards [18, 19] and were compared with results of unaged specimens reported previously by the authors [14].

The second set of tests was conducted on modified DCB and SLB specimens (see Fig. 1b and 1c), and the results were used to evaluate the degradation of the interfaces of the glass/steel connections for the two adhesives used in this study. The tests were conducted adopting the methodology described in previous research by the authors [15], and the results were compared to identical unaged specimens. An evaluation of the effect of the exposure conditions considered for shorter periods was also performed utilising the DCB specimens by testing them after 1, 2 and 3 weeks. SLB tests were performed for 3 weeks of exposure only. Also, exposure of the DCB specimens to an elevated temperature at 45 °C without water immersion was performed to evaluate the effects of thermal degradation only, and to determine the dominant parameters for interface joint degradation.

The third set of tests was conducted on large scale double lap shear joints (see Fig. 2). The results were once again compared to identical tests on unaged specimens previously reported by the authors [14, 15]. The designs of the three sets of tests can be found in Figures 1 and 2, while Table 1 presents the matrix of tests performed for each adhesive. The bondline thickness of 0.2 mm was kept constant for all tests.

For the DCB/SLB specimens and the larger scale adhesive joints, the steel substrates were sandblasted initially and afterwards degreased with acetone, while the glass substrates were only degreased with acetone. Atmospheric plasma treatment with a mixture of argon and oxygen was used on both the glass

and steel substrates immediately prior to adhesive application to improve surface activation. The bonding took place at room temperature as per manufacturers' recommendations. The adhesives were not degassed before bonding, and it is therefore possible that small voids or imperfections were present in the bond zone. However, visual inspections during manufacture and after curing did not reveal any significant defects.

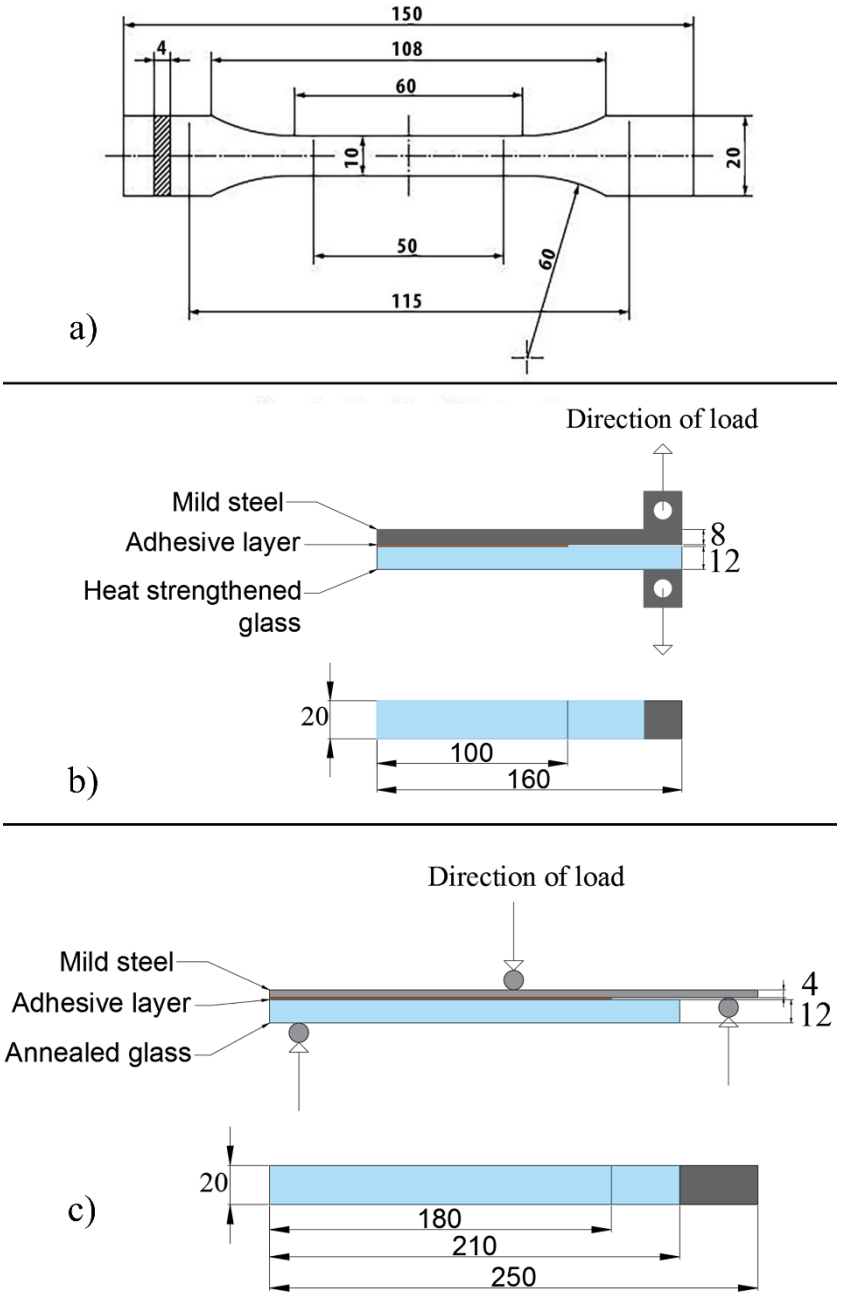

Figure 1: Designs for a) dogbone, b) DCB and c) SLB specimens. Dimensions in mm.

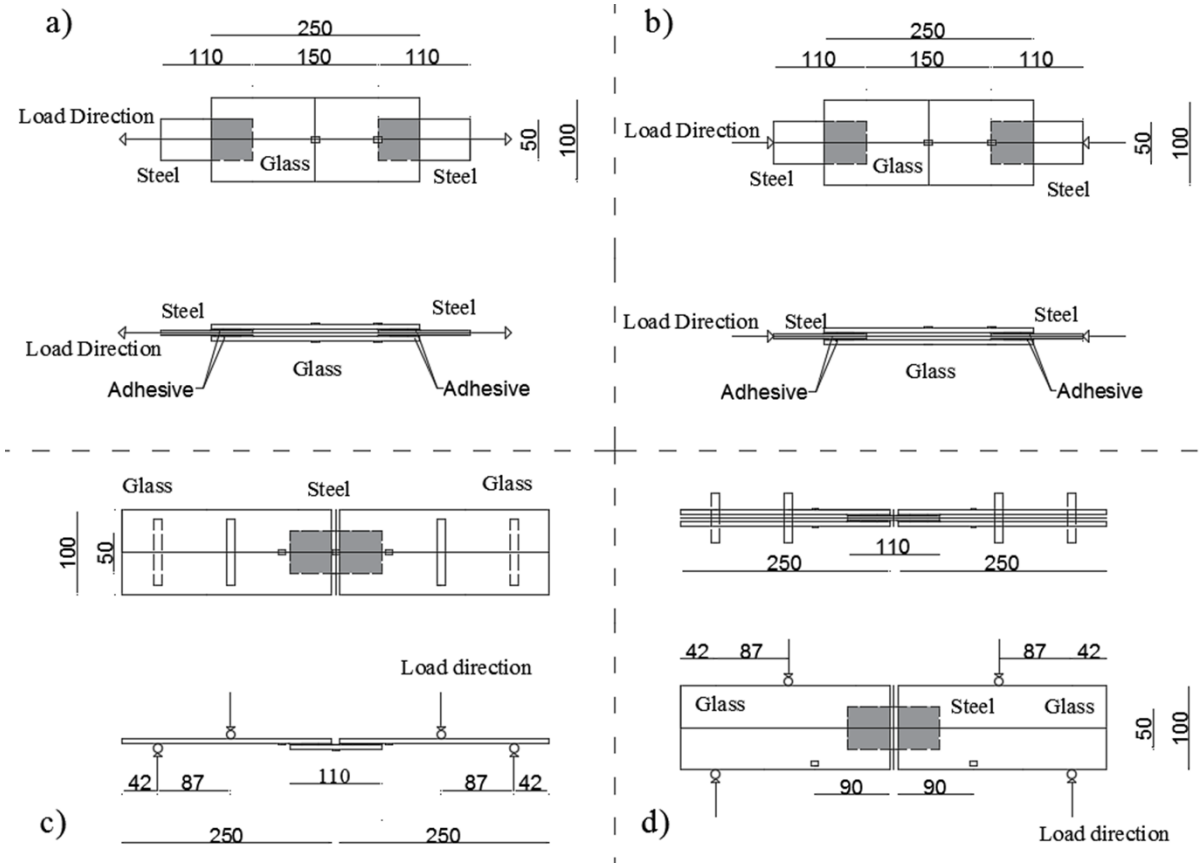

Figure 2: Design details for evaluation of uniaxial a) tension and b) compression, c) out-of-plane and d) in-plane bending loading conditions. Locations of strain gauges are indicated. Dimensions in mm.

Table 1: Test matrix for each adhesive

Specimen Type	Loading	Conditions			Number of tests
		Heat (45 °C)	Humidity (100%)	Duration (Weeks)	
Dogbone		Yes	Yes	3	5
DCB		Yes	No	1	5
DCB		Yes	Yes	1	5
DCB		Yes	Yes	2	5
DCB		Yes	Yes	3	5
SLB		Yes	Yes	3	5
Double lap-shear joint	Uniaxial tension	Yes	Yes	3	4
	Uniaxial compression	Yes	Yes	3	4
	Out-of-plane bending	Yes	Yes	3	4
	In-plane bending	Yes	Yes	3	4

2.5 Numerical predictive methodology

Two different numerical methodologies were established for the analysis of the double lap shear joints. The first is based on a Continuum Mechanics (CM) approach by coupling a linear Drucker-Prager yield criterion (equation 1) to a ductile damage failure model [20] for the damage initiation and propagation of the adhesive layer.

$$t - p\tan\beta = d \tag{1}$$

In equation (1), t is the effective stress, p is the hydrostatic pressure stress, $\tan\beta$ is the pressure sensitivity factor while d is a material property related to the yield stress in pure shear. Figure 3a shows a graphical representation of the Drucker-Prager model that was used in the analysis. For the ductile damage failure model, the fracture strain, as a function of the triaxiality factor, is evaluated against the critical fracture strain. Once the fracture strain reaches the critical value (for different triaxiality values) the damage initiates in the adhesive layer. This methodology is described in detail in [14] and formulas for all parameters can be found there. The properties for the definition of the constitutive models were based on the mechanical properties of the adhesives determined by tests on tensile dogbones (see Table 2). The bulk properties can be found in Table 2 while the hardening curves are extracted from Figure 3. The pressure sensitivity factor required for the Drucker Prager model and Poisson's ratio were assumed to remain unchanged after environmental exposure and can be found in [14, 15].

The second methodology is based on a Cohesive Zone Modelling (CZM) approach, which is described in detail in [15]. The properties for the traction-separation or cohesive laws were obtained from the interface characterization tests by performing inverse analysis on test results for both the DCB and SLB specimens. A simple triangular cohesive law was assumed for the numerical fitting. The damage initiation was introduced using a quadratic nominal stress criterion while an energy criterion based on linear elastic fracture mechanics was used for damage propagation as shown in equations 2 and 3 [15]. The respective properties are given in Tables 5 and 6.

$$\left(\frac{t_n}{t_n^c}\right)^2 + \left(\frac{t_s}{t_s^c}\right)^2 = 1 \tag{2}$$

$$\frac{G_n}{G_n^c} + \frac{G_s}{G_s^c} = 1 \tag{3}$$

In equation (2), t_n and t_s are the stresses corresponding to fracture opening modes I and II, while t_n^c and t_s^c are values for the critical traction for tension and shear, respectively. Similarly, in equation (3) G_n and G_s are the fracture energies corresponding to modes I and II, while G_n^c and G_s^c are the critical

fracture energies for pure tension and shear, respectively. Therefore, the damage initiates when the critical traction is reached while the elements fail completely and are removed from the analysis when the critical fracture energy G^c (or critical displacement δ^c) is reached. Figure 3b shows a graphical representation of the triangular cohesive law that was used for the CZM methodology.

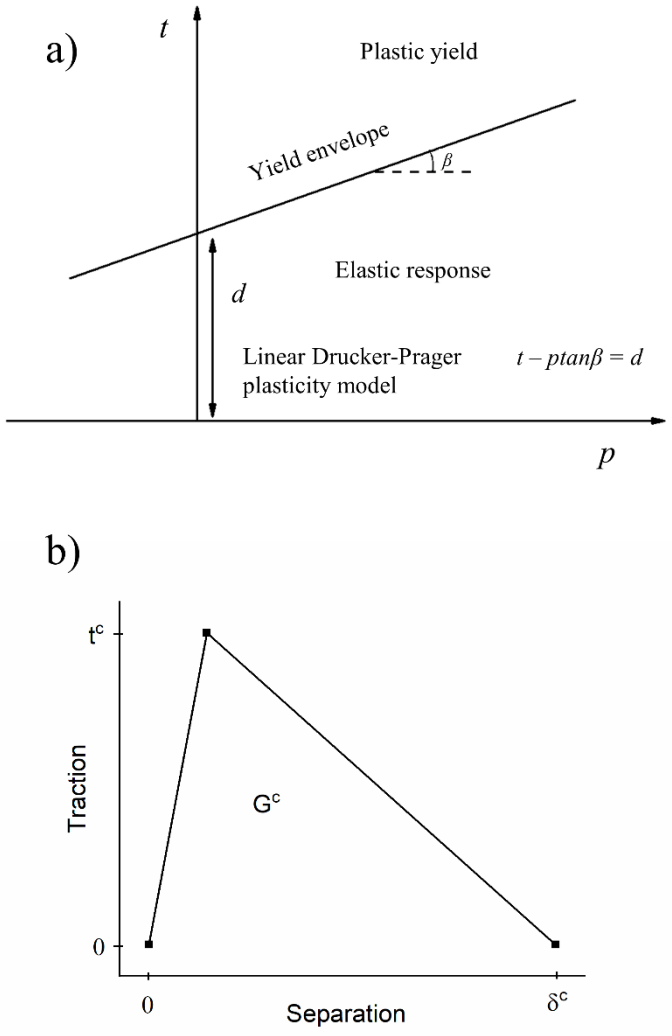

Figure 3: Graphical representation of a) the linear Drucker Prager yield criterion used for the CM methodology and b) the triangular traction-separation used for the CZM methodology

The damage in the glass substrate was also considered by introducing a brittle cracking model as in [14]. For the numerical analyses, the commercial Finite Element (FE) software ABAQUS Explicit (v6.14) was used. 3D stress, 8-node linear solid elements (C3D8R) with reduced integration and hourglass control were used for the continuum mechanics approach, while 8-node three-dimensional cohesive elements (COH3D8) were utilised for the elements representing the cohesive zone.

3 Results and Discussion

3.1 Bulk property degradation

Figure 4 shows characteristic measured stress-strain responses while the key mechanical properties are summarised in Table 2. The stress-strain curves and the mechanical properties of the unaged specimens, reported in a previous publication by the authors [14], are used here to establish the degree of property degradation and are also presented. Slight colour changes were observed for both adhesives after the exposure.

Table 2 shows that the brittle adhesive was damaged less by the environmental exposure based on the relative changes for the elastic modulus, tensile yield and failure strain. The elastic modulus reduced by 27%, compared to a 39% reduction observed for the ductile adhesive. The yield and failure stress followed similar trends with the brittle adhesive properties reducing 11% and 8%, respectively, while the respective reductions recorded for the ductile adhesive were 63% and 30%. Finally, it should be noted that the elongation (strain-to-failure) for both adhesives increased by 41% and 46%, respectively. Similar trends (reduction of strength and increase of ductility) are reported in relevant studies [5, 12].

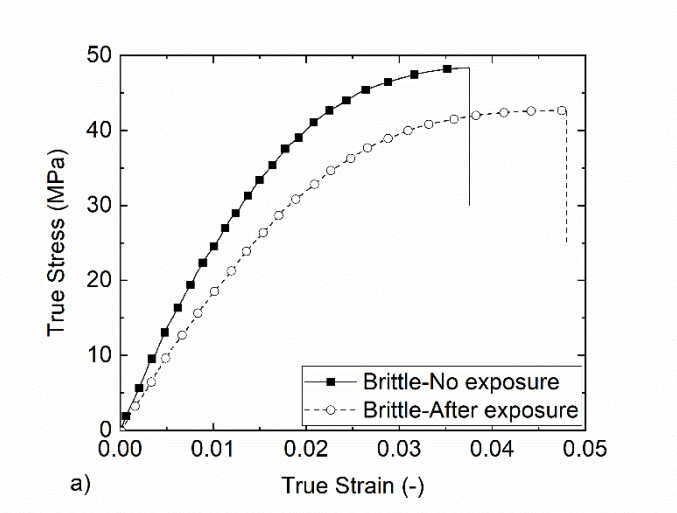

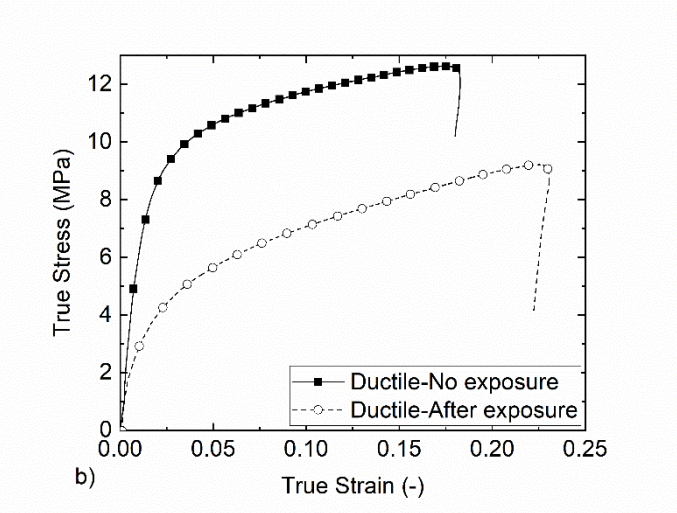

Figure 4: Characteristic stress-strain curves for the a) Araldite 2020 (brittle) and b) Araldite 20147-1 (ductile) adhesive before and after exposure of 3 weeks in water at 45 °C.

Table 2: Mechanical bulk adhesive properties before and after exposure of 3 weeks in water at 45 °C.

	Araldite 2020 (before exposure)	Araldite 2020 (after exposure)	Property change (%)	Araldite 2047-1 (before exposure)	Araldite 2047-1 (after exposure)	Property change (%)
Young's modulus (E), GPa	2.57 ± 0.08	1.87 ± 0.21	-27	0.89 ± 0.08	0.54 ± 0.05	-39
Tensile yield strength (σ_{yT}), MPa	31.33 ± 2.73	27.88 ± 4.04	-11	5.56 ± 0.11	2.03 ± 0.30	-63
Tensile failure stress (σ_{fT}), MPa	45.39 ± 2.61	41.66 ± 1.00	-8	13.10 ± 1.13	9.17 ± 0.50	-30
Tensile failure strain (ε_{fT}), %	3.1 ± 0.6	4.37 ± 0.73	41	17 ± 4.1	24.89 ± 3.65	46

3.2 Effect of exposure on glass/steel interfaces

3.2.1 Interface degradation

The modified DCB/SLB samples were used to determine the outcome of introducing environmental exposure conditions on the strength of the glass/steel bonded interfaces. The geometry of the DCB/SLB samples is smaller and thus the specimens are more cost-effective in terms of manufacturing compared to the large double lap shear joints and can lead to a quicker evaluation of the effect of the environmental conditions. Therefore, shorter exposure periods were also studied. Also, the DCB/SLB samples can be

used for the extraction of cohesive laws for the exposed interfaces and as a result can provide necessary input data to numerically simulate the degradation of the double lap adhesive shear joints. Additional details for the testing methodology of the DCB/SLB specimens can be found in [15].

Figure 5 shows the characteristic load-displacement curves obtained for the DCB specimens after 1, 2 and 3 weeks of combined humidity and elevated temperature, as well as 1 week of thermal exposure only for both adhesives. Besides, unaged specimen results [15] are also included for benchmarking purposes.

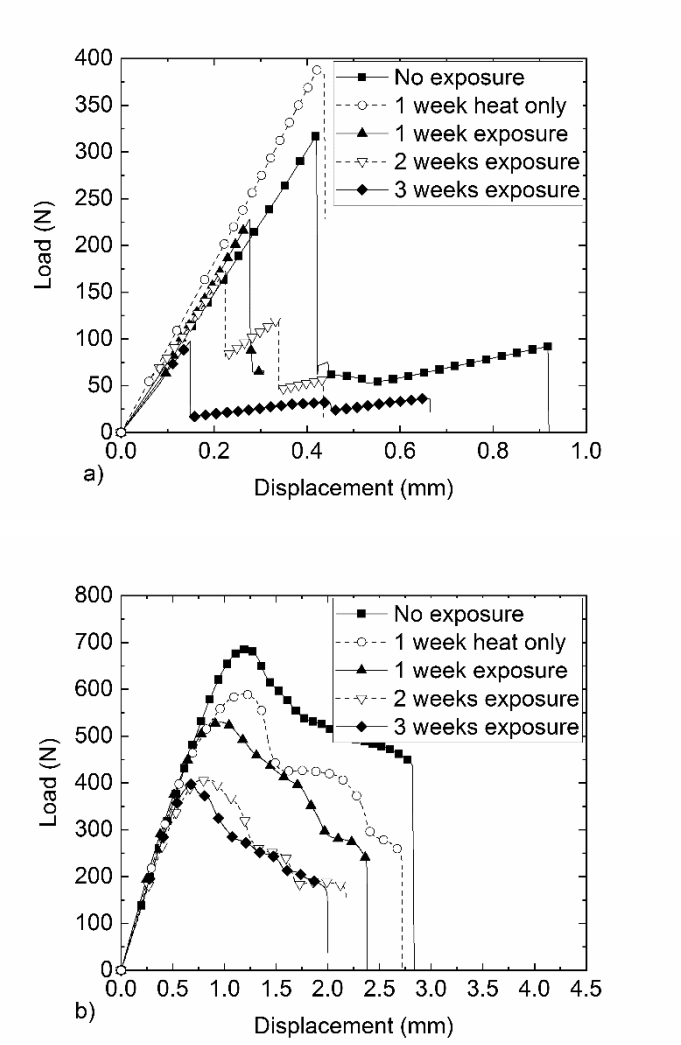

Figure 5: Characteristic load-displacement curves recorded for the a) Araldite 2020 (brittle) and b) Araldite 2047-1 (ductile) DCB specimens for no exposure and 1, 2, 3 weeks of exposure.

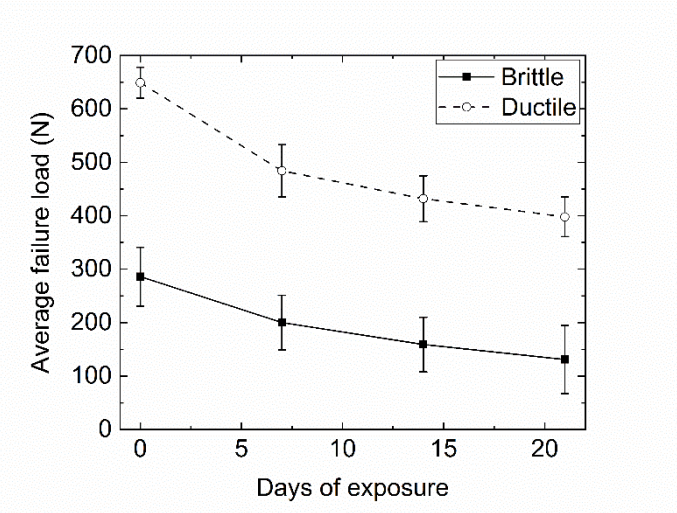

Figure 6: Average failure load of the DCB specimens as a function of exposure time.

The results of the testing of the modified DCB specimens are summarised in Table 3. Figure 6 visualises the reduction of the average maximum load of the DCB specimens as a function of time for both adhesives. In line with typical moisture uptake curves and relevant studies (e.g. [21]), the damage is more severe in the early stages of exposure and afterwards gradually slows down. After 3 weeks of exposure, the maximum load recorded for the brittle DCB specimens reduced 55% while the respective reduction for the ductile DCB specimens was 39%. Interestingly, the damage is less severe for the ductile DCB specimen compared to the brittle ones, reversing the trend observed for the bulk properties of the adhesives.

Also, it is shown that the elevated temperature only exposure had a small effect on the ductile adhesive reducing its maximum load capacity by 14%. For the brittle adhesive, the additional temperature exposure was shown to even lead to an increase of strength of 18%, which was attributed to additional post-curing of the resin. However, it should be noted that the coefficient of variation also increased significantly with longer exposure times, especially for the brittle adhesive.

Table 3: Summary of the experimental testing results for the DCB specimens

Exposure condition	Adhesive type	Average maximum load (N)	Coefficient of variation (%)
No exposure	Araldite 2020 (brittle adhesive)	286 ± 55	19.2
1 week - at 45 °C		337 ± 54	16.0
1 week of water immersion at 45 °C		200 ± 51	25.5
2 weeks of water immersion at 45 °C		159 ± 51	32.1
3 weeks of water immersion at 45 °C		131 ± 64	48.9
No exposure	Araldite 2047-1 (ductile adhesive)	649 ± 29	4.5
1 week at 45 °C		559 ± 45	8.1
1 week of water immersion at 45 °C		484 ± 49	10.1
2 weeks of water immersion at 45 °C		432 ± 43	10.0
3 weeks of water immersion at 45 °C		398 ± 37	9.3

The interfaces of the ductile DCB specimens after failure for exposure periods of 1, 2 and 3 weeks are shown in Figure 7. The moisture ingress can be identified by the different adhesive colour close to the sides of the specimens. Stress whitening development during testing was observed in the unaffected part of the adhesive layer as previously reported by the authors in studies with the same adhesive [14, 15]. The prevailing failure mode was adhesive (interfacial) on the glass side. The size of the affected areas due to moisture ingress increased from 25% to 37% after one and three weeks of exposure periods, respectively. These observations are in line with the observed reduction of the load capacity of the DCB specimens for the same exposure periods. The degradation mechanism observed for the brittle adhesive was different. Here, the moisture ingress could not be identified visually as no strain whitening could be observed during testing. The mode of failure was 100% adhesive (interfacial) on the glass side and the reduction of the load capacity of the specimens was the only indication of the effect of environmental exposure.

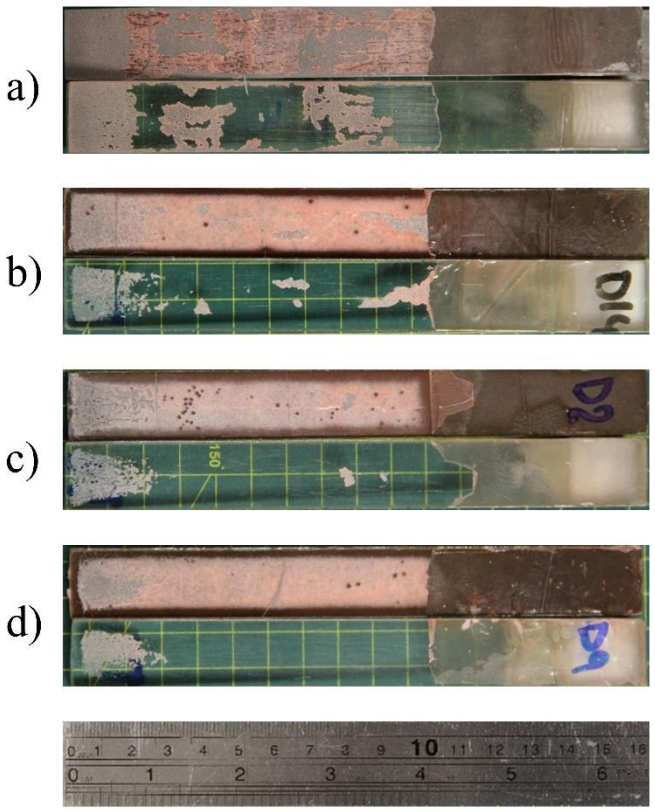

Figure 7: Observed interface failure of the DCB specimens for the Araldite 2047-1 (ductile) adhesives after a) no exposure, b) 1 week, c) 2 weeks and d) 3 weeks of exposure.

The SLB specimen testing was limited to three weeks of exposure, and characteristic load-displacement curves are shown in Figure 8 including the reference unaged specimens for comparison purposes. Also, the resulting degradation of the specimens after 3 weeks of exposure is presented in Table 4 while the specimens after testing are shown in Figure 9. A moisture ingress ring was observed for the ductile SLB specimens and was similar to the one observed for the ductile DCB specimens. A similar effect could also be seen for the brittle SLB specimens under mixed-mode testing. It should be noted that the brittle and ductile SLB specimens recorded strength reductions of 26% and 15% compared to identical unaged specimens, which was significantly lower compared to the respective 55% and 39% reduction recorded for the DCB specimens for the same exposure time. It can therefore be assessed that the resistance to the peel stresses developed for fracture opening mode I is more sensitive to environmental degradation, as compared against the resistance to the shear stresses developed for mode II. As before, the coefficient of variation increased significantly with the exposure.

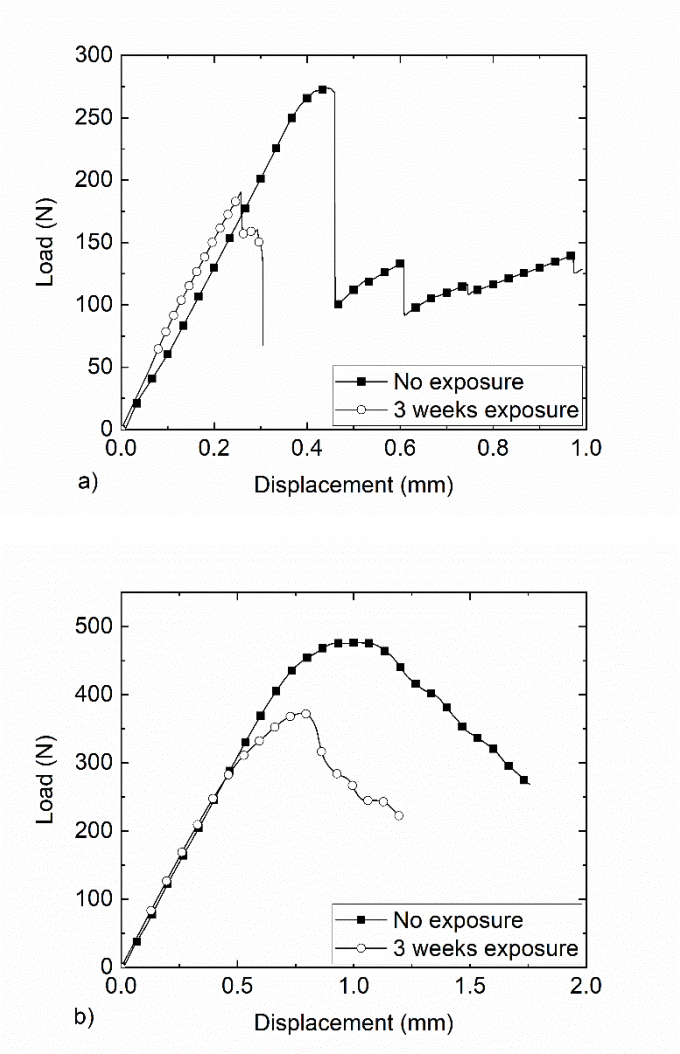

Figure 8: Characteristic load-displacement curves for the a) Araldite 2020 (brittle) and b) Araldite 2047-1 (ductile) SLB specimens for no exposure and three weeks of exposure.

Table 4: Summary of the experimental testing for the SLB samples under exposure.

Exposure condition	Adhesive type	Average maximum load (N)	Coefficient of variation (%)	Property change (%)
No exposure	Araldite 2020 (brittle adhesive)	254 ± 21	8.3	-26
3 weeks of water immersion at 45 °C		188 ± 51	27.1	
No exposure	Araldite 2047-1 (ductile adhesive)	419 ± 45	10.7	-15
3 weeks of water immersion at 45 °C		355 ± 62	17.5	

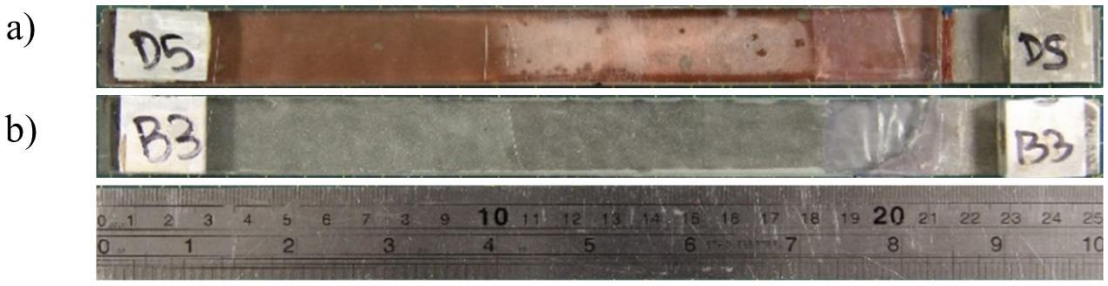

Figure 9: Observed interface failure of the SLB specimens for the a) Araldite 2020 (brittle) and b) Araldite 2047-1 (ductile) adhesives after 3 weeks of exposure.

3.2.2 Numerical input parameters

For the calibration of the traction separation laws after exposure the inverse FE method, as described by da Silva and Campilho [22] was employed. Firstly, the traction and fracture energy under mode I were calibrated utilising the DCB experimental data and secondly, the properties under mixed mode were also extracted utilising the SLB experimental data [15].

Figure 10 shows experimental load-displacement curves for the DCB specimens for no environmental exposure and three weeks of exposure. The subsequent achieved numerical fitting is also displayed for both adhesives. The shaded areas represent the experimental variation and are bound by the maximum and minimum measured experimental curves. One experimental curve representing average interface stiffness and strength was selected for the numerical fitting.

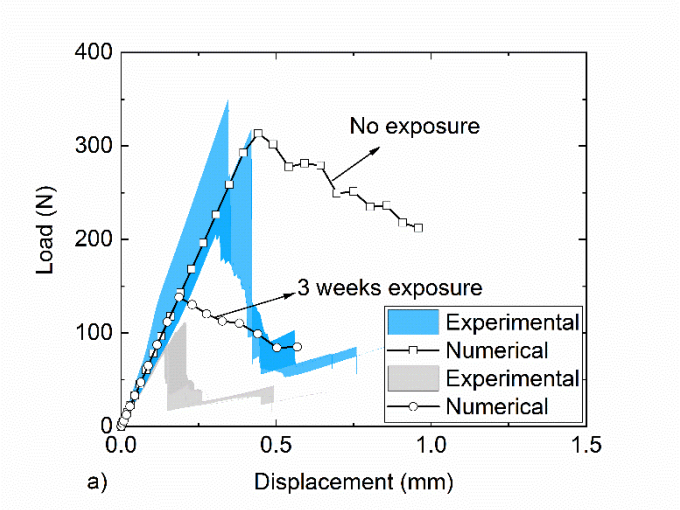

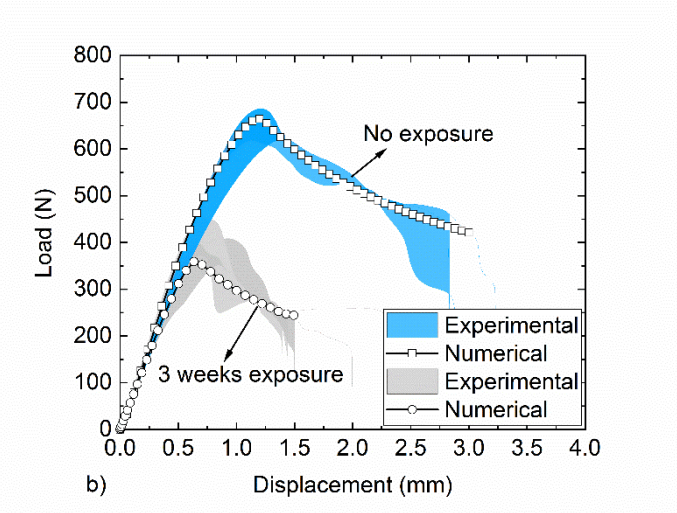

Figure 10: Experimental load-displacement curve variation for the a) Araldite 2020 (brittle) and b) Araldite 20147-1 (ductile) DCB samples and numerical curve fitting of the CZM prediction for no environmental exposure and 3 weeks of exposure.

Table 5: Calibrated cohesive model properties for fracture opening mode I before and after environmental exposure for the Araldite 2020 (brittle) and Araldite 2047-1 (ductile) adhesives.

	Araldite 2020 (brittle adhesive)		Araldite 2047-1 (ductile adhesive)	
Property	Before exposure	After exposure	Before exposure	After exposure
E (GPa)	2.57	1.87	0.89	0.54
t_n^c (MPa)	25	12	10	8
δ_n^c (mm)	0.004	0.004	0.104	0.075
G_n^c(J/m^2)	50	25	520	300

Table 5 summarises the calibrated model parameters for the two adhesives before and after environmental exposure. A moderate reduction is reported for both the tractions and the fracture energies of the two adhesives. The ductile adhesive is affected less by the environmental exposure retaining 80% of the initial traction and 60% of the initial fracture toughness after exposure. The respective values for the brittle adhesive are 50% for both the traction and the fracture energy. It is worth noting, however, that the larger coefficient of variation observed for the exposed DCB specimens increased the uncertainty of the parameter fit between the experimental data and the FE input data during the inverse fitting process.

Figure 11 shows the experimental load-displacement curves for the SLB specimens for no environmental exposure and three weeks of exposure. The subsequent numerical fitting achieved is also displayed for both adhesive types. Again, the shaded areas represent the experimental variation and are bound by the maximum and minimum measured experimental curves while one experimental curve representing average interface stiffness and strength was selected for the numerical fitting.

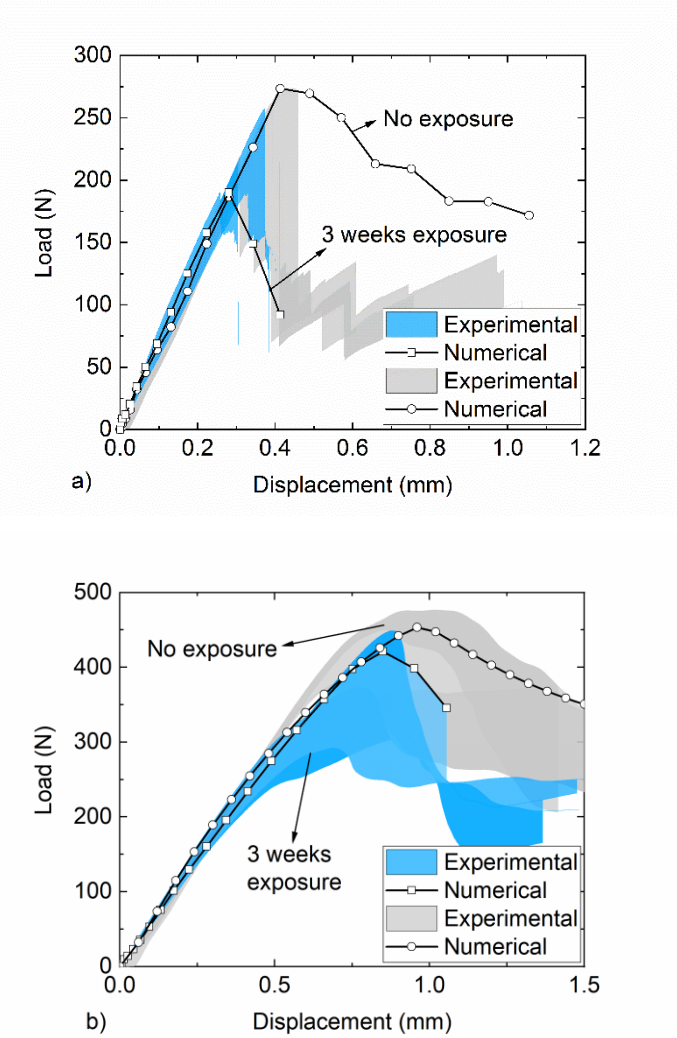

Figure 11: Experimental load-displacement curve variation for the a) Araldite 2020 (brittle) and b) Araldite 2047-1 (ductile) SLB samples and numerical curve fitting for the CZM material law for no environmental exposure and 3 weeks of exposure.

Table 6: Calibrated cohesive properties for fracture opening mode II before and after environmental exposure for the Araldite 2020 (brittle) and Araldite 2047-1 (ductile) adhesive.

	Araldite 2020 (brittle adhesive)		Araldite 2047-1 (ductile adhesive)	
Property	Before exposure	After exposure	Before exposure	After exposure
G (GPa)	0.93	0.67	0.31	0.19
t_s^c (MPa)	15	6	2	2
δ_s^c (mm)	0.013	0.05	1.04	0.5
G_s^c (J/m^2)	100	150	1040	500

Table 6 summarises the calibrated model properties for the two adhesives before and after environmental exposure corresponding to fracture opening mode II. The properties of the traction-separation law in mode II also degraded, with the only exception being the fracture energy of the brittle

adhesive, which increased slightly. The small increase can be explained by the enhanced ductility of the brittle adhesive as per the bulk property determination. As observed for the DCB specimens, the larger experimental scatter, increased the uncertainty of the parameter fit during the calibration stage.

Based on the tests conducted on bulk adhesive materials, it was anticipated that the initiation stress and fracture energy of the cohesive laws would reduce. The critical displacement of the triangular cohesive law was expected to increase to reflect the subsequent rise in the ductility (strain-to-failure) of both adhesives. Such observations were made for the brittle adhesive under mode II loading (Table 6), but not for the other tests. It is noted here that the selected triangular cohesive law might oversimplify the response of the interfaces, especially when considering the enhanced ductility after environmental degradation. Trapezoidal shapes like the ones used by Campilho et al. [23], provide a stress plateau and therefore could be more representative for adhesives with increased ductility. Besides, it is likely that other combinations of traction and fracture energy could also capture the experimental response observed in the DCB/SLB specimens for the two adhesives. Finally, it can be speculated that a direct measurement of the cohesive laws from DCB/SLB specimens as reported by other research groups (e.g. Sorensen [24] and Carlberger and Stigh [25]) could further improve the confidence in the data derivation and the accuracy of the predictions, but this was not attempted in this research due to time constraints.

3.3 Analysis and prediction of double lap shear adhesive joints after environmental exposure

3.3.1 Experimental degradation

In this section, the mechanical response and failure performance of the double lap adhesive shear joints is presented. The joints were exposed to the environmental conditions described in section 2.1 for 3 weeks. The load cases for which the joints were tested are explained in section 2.2. A minimum of 4 specimens were tested for each load case. Comparisons with identical unaged joints, presented in earlier publications by the authors [14], are also presented.

A summary of the tests under uniaxial tensile and compressive loading is presented in Table 7, while a summary of the tests under in-plane and out-of-plane loading is presented in Table 8. Tables 7 and 8 include information about the failure loads and mechanisms observed experimentally and compare the respective performance of the joints before and after exposure. The load capacity of all types of joints reduced significantly ranging from 29% to 48%. Failures mostly initiated at the interfaces but in some cases, this led to sudden unbalancing of the joints and created stress waves that caused a dynamic fracture of the glass substrates. Overall, the failure mechanisms remained unchanged.

Table 7: Summary of measured data from uniaxial tests for Araldite 2020 (brittle) and Araldite 2047-1 (ductile) adhesive joints before and after environmental exposure

		Before exposure		After exposure		Percentage change (%)
Load case	Adhesive type	Failure load (kN)	Failure mechanism	Failure load (kN)	Failure mechanism	
Tensile loading	Brittle	38.0 ± 1.8	Significant damage in the adhesive layer/interface leading to glass failure	21.4 ± 1.5	Significant damage in the adhesive layer/interface leading to glass failure	-44
	Ductile	46.7 ± 4.5	Cohesive failure	34.2 ± 5.7	Adhesive/cohesive failure	-27
Compressive loading	Brittle	42.4 ± 5.1	Significant damage in the adhesive layer/interface leading to glass failure	29.7 ± 4	Significant damage in the adhesive layer/interface leading to glass failure	-30
	Ductile	46.2 ± 0.6	Cohesive failure	34.6 ± 5.5	Adhesive/cohesive failure	-25

Table 8: Summary of measured data from the bending tests for Araldite 2020 (brittle) and Araldite 2047-1 (ductile) adhesive joints before and after environmental exposure

		Before exposure		After exposure		Percentage change (%)
Load case	Adhesive type	Failure load (kN)	Failure mechanism	Failure load (kN)	Failure mechanism	
Out-of-plane bending loading	Brittle	0.83 ± 0.21	Adhesive / cohesive failure	0.42 ± 0.03	Damage initiation in the adhesive layer leading to glass failure	-49
	Ductile	1.45 ± 0.04	Glass failure	1.05 ± 0.16		-28
In-plane bending loading	Brittle	14.3 ± 0.7	1) Adhesive / cohesive failure 2) Glass failure preceded by significant damage in the adhesive layer	7.85 ± 1.25	Glass failure	-45
	Ductile	20.0 ± 0.4		13.8 ± 3.5	1) Adhesive / cohesive failure 2) Glass failure preceded by significant damage in the adhesive layer	-31

Figures 12, 13 and 14 show the interfaces of the double lap shear adhesive joints after failure. The moisture ingress was evident for the ductile adhesive joints in a very similar way as for the DCB and SLB specimens. The central parts of the joint that were not influenced by the moisture ingress developed stress whitening in the same manner as the unaged adhesive joints.

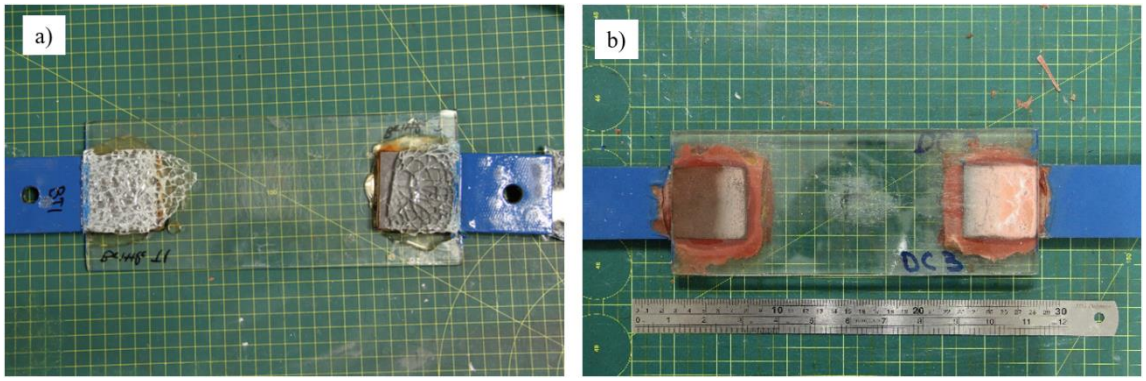

Figure 12: Characteristic glass/steel interfaces after failure for a) Araldite 2020 (brittle) and b) Araldite 2047-1 (ductile) joints subjected to uniaxial loading. All bonded overlap regions are 50 mm x 50 mm.

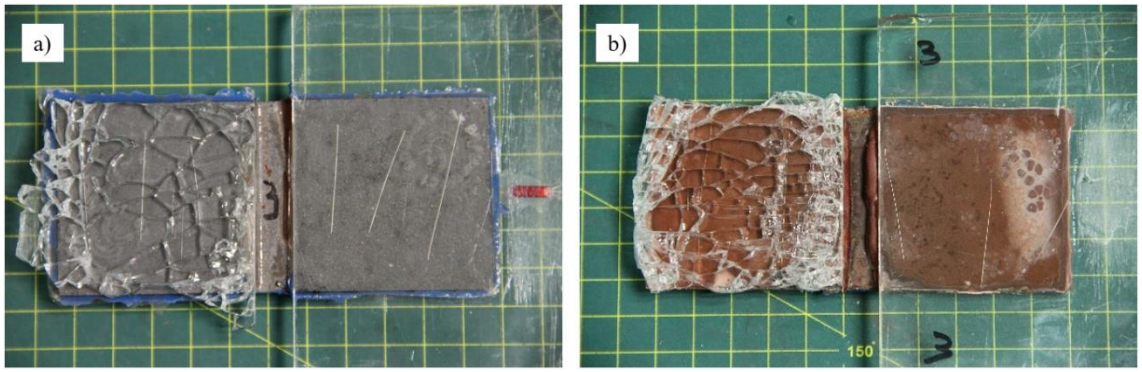

Figure 13: Characteristic glass/steel interfaces after failure for a) Araldite 2020 (brittle) and b) Araldite 2047-1 (ductile) joints subjected to out-of-plane bending loading. All bonded overlap regions are 50 mm x 50 mm.

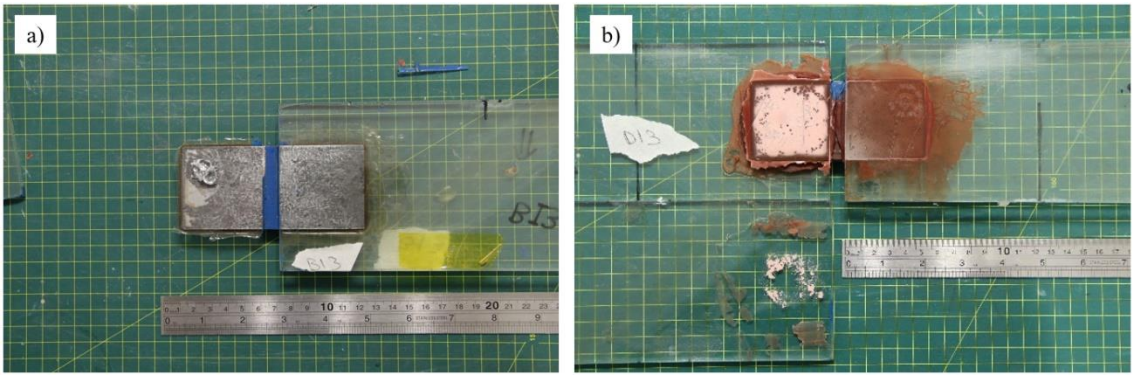

Figure 14: Characteristic glass/steel interfaces after failure for a) Araldite 2020 (brittle) and b) Araldite 2047-1 (ductile) joints subjected to in-plane bending loading. All bonded overlap regions are 50 mm x 50 mm.

The focus of the present study is the evaluation of the two different numerical methodologies regarding their respective ability to predict damage and failure in glass/steel adhesive joints after environmental exposure. This discussion will shed light on the dominating failure mechanism of bulk versus interface degradation in adhesive joints under environmental exposure, which is generally difficult to determine experimentally.

At the same time, it is nevertheless considered appropriate to also add an interpretation of the experimental performance of the joints based on the ETAG 002 guideline. The most relevant criterion for the exposure conditions considered is 6.1.4.2 (Residual strength after artificial ageing). According to the ETAG 002 methodology, there are two conditions that need to be satisfied. The first requirement is that the joints retain 75% of their initial strength following exposure. For the adhesives studied, the brittle joints retained around 50% of their initial strength for all load cases, while the ductile joints retained about 70-75% for all load cases. The second criterion is related to the mode of failure with the requirement to have a minimum of 90% cohesive failure. For the brittle adhesive, the damage was characterised as almost entirely adhesive and for the ductile adhesive it was mixed (but less than 90% cohesive). It is worth noting however, that these two adhesives did not display entirely cohesive failure before environmental exposure either. Therefore, following the interpretation of the ETAG 002 guideline, the two adhesives did not meet the required criteria.

3.3.2 Numerical prediction

Table 9 assesses the respective ability of the two modelling methodologies described in Section 2.4, namely Continuum Mechanics (CM) and Cohesive Zone Modelling (CZM), to predict damage initiation and failure in glass/steel adhesive joints under the four different experimental load cases. This is achieved by comparing the numerically predicted failure loads with the experimental observations. The highlighted cells indicate which method results in the best agreement with the experimental data.

Table 9: Evaluation of the numerical predictions of the failure loads, using the two different modelling methodologies to predict the failure load of Araldite 2020 (brittle) and Araldite 2047-1 (ductile) adhesive joints after environmental exposure

	Failure loads for the Araldite 2020 (brittle) adhesive			Failure loads for the Araldite 2047-1 (ductile) adhesive		
	Experimental (kN)	CM (kN)	CZM (kN)	Experimental (kN)	CM (kN)	CZM (kN)
Tension	21.4 ± 1.5	40.5	**27.2**	34.2 ± 5.7	**29.5**	**29.9**
Compression	29.7 ± 4	47.7	**27.2**	34.6 ± 5.5	**29.6**	**29.9**
Out-of-plane bending	0.42 ± 0.03	1.13	**0.58**	1.05 ± 0.16	**1.34**	**1.33**
In-plane bending	8.78 ± 1.41	15.9	**10.4**	13.83 ± 3.49	**14.4**	12.6

For the brittle adhesive, significant differences were observed between the experimental observations and the predicted failure load utilising the CM approach. The inability of the CM approach to capture the degradation of the joints is because the damage is adhesive (interfacial) and thus could not be captured by simply reducing the bulk properties of the adhesive. The CZM approach, in contrast, has a better agreement with the experimental data as it also captures interface degradation through its input data, even though it still somewhat overestimates the failure loads.

For the ductile adhesive, both CM and CZM methodologies can accurately predict the performance of the joints after environmental exposure. Because the CM approach assumes cohesive damage (i.e., failure is entirely dependent on the bulk properties of the adhesive), it can be determined that the damage in the ductile adhesive joints is mostly due to the degradation of the bulk properties of the adhesive and to a lesser extent due to the damage in the interface. This agrees with the experimental observation. The failure mechanism is mostly cohesive, leading the adhesive to yield and develop a large plastic zone, as displayed by the stress whitening observed. Lastly, it is noted that the two methodologies can only agree if the CZM methodology also successfully captures both adhesive and cohesive damage via its input parameters.

Given the above conclusions, it becomes obvious that joint predictions involving potentially both interface and bulk adhesive degradation require a CZM-type approach to enable accurate prediction. The more complex input parameter derivation is considered worthwhile given the ability to capture both failure modes with and without environmental exposure with the same modelling approach. For the remaining numerical studies and analyses, the CZM methodology will be used.

3.3.2.1 Numerical prediction of uniaxial loading response and property degradation

Figures 15 and 16 correlate the load with the strain recorded in the midpoints of the joints for uniaxial tensile and compressive loading. The graphs also include the numerical predictions for the load-strain relationships as predicted by the CZM methodology. The evaluation of the strain response was based on strain gauge measurements and FE predictions at the midpoints of the joints. The responses of the unaged joints were also included in the figures for comparison. Additionally, the figures provide information for the predicted load at damage initiation for both cases.

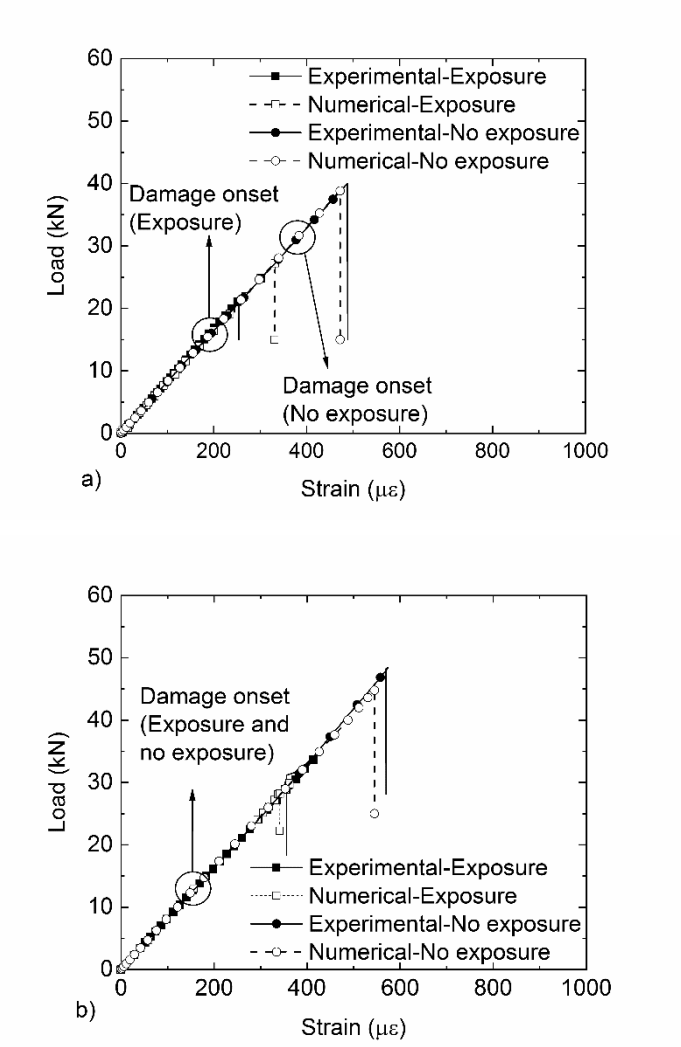

Figure 15: Characteristic strain-load response at the midpoints of the a) Araldite 2020 (brittle) and b) Araldite 2047-1 (ductile) adhesive joints subjected uniaxial tensile loading. Numerical results represent predictions by the CZM methodology.

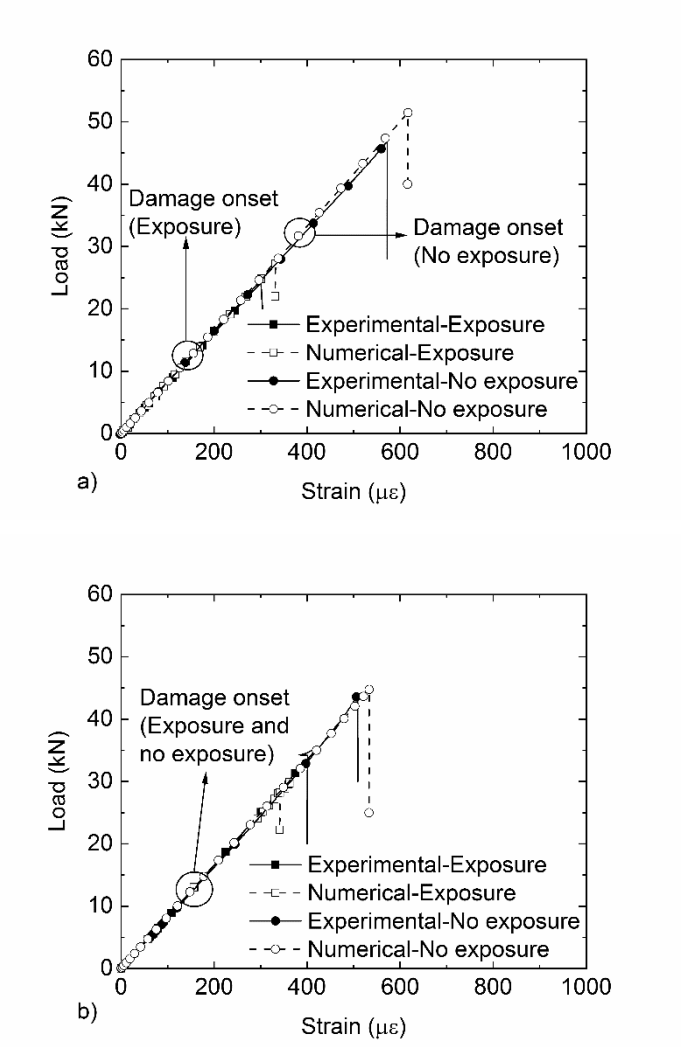

Figure 16: Characteristic strain response at the midpoints of the a) Araldite 2020 (brittle) and b) Araldite 2047-1 (ductile) adhesive joints subjected to uniaxial compressive loading with and without environment exposure. Numerical results represent predictions by the CZM methodology.

Considering the strain responses, the experimental observations and numerical predictions show very good agreement. It should be noticed that the numerical predictions for the brittle adhesive joints overestimated the failure load by 24% for tensile loading, and slightly underestimated the failure load for compression loading by 8%. Moreover, the numerical predictions for the ductile adhesive joints underestimated the failure loading capacity for both tensile and compressive loading by about 14%. The numerical predictions in most cases were within the experimental scatter but it is worth noting that the standard deviations of the environmentally aged joints were significantly higher compared to the unaged ones.

3.3.2.2 Numerical prediction of bending loading response and property degradation

Figures 17 and 18 correlate the load with the strain recorded for environmentally aged joints subjected to out-of-plane and in-plane bending. The evaluation of the strains took place in the areas of glass stress concentrations for the two types of joints (as discussed in [14]). The responses of the unaged joints are also included in the figures for comparison purposes. The figures also provide information for the predicted load at damage initiation for both cases.

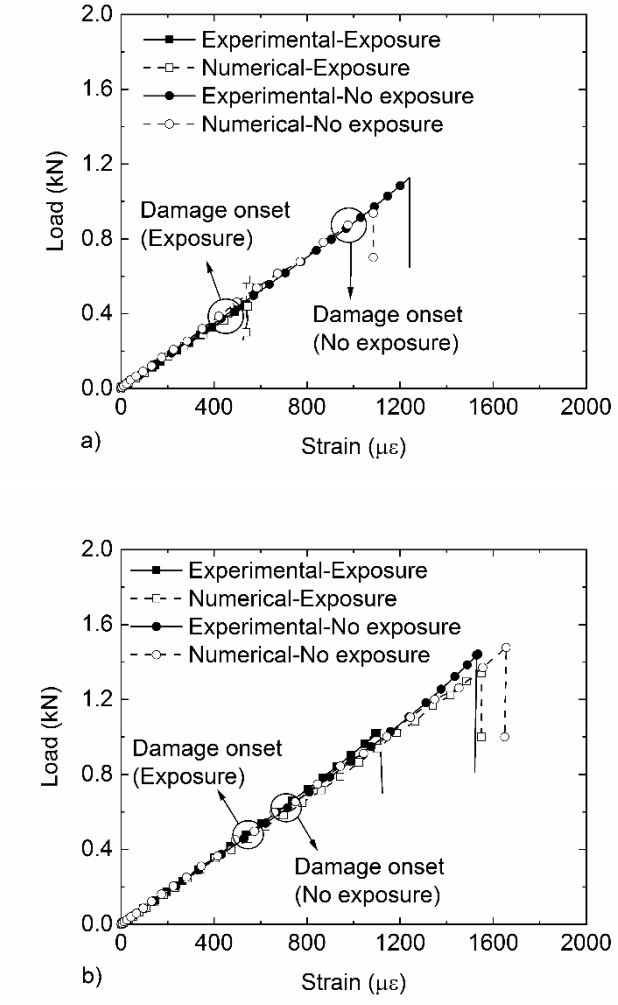

Figure 17: Characteristic strain-load response in the areas of stress concentrations of the a) Araldite 2020 (brittle) and b) Araldite 2047-1 (ductile) adhesive joints subjected to out-of-plane bending loading with and without environment exposure. Numerical results for joints represent predictions by the CZM methodology.

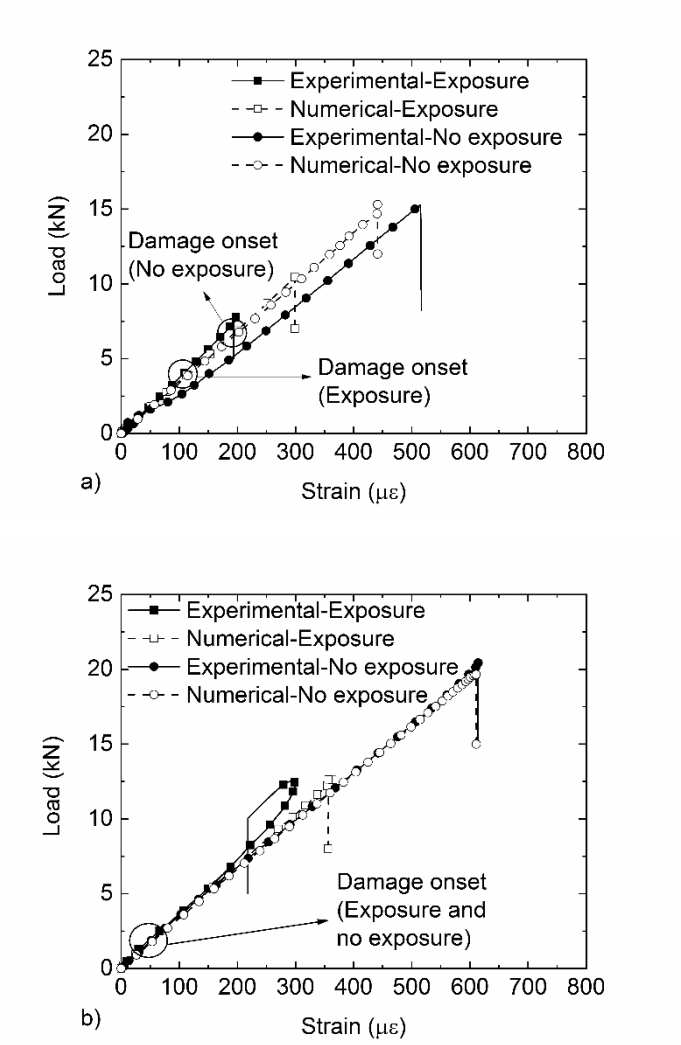

Figure 18: Characteristic strain-load response in the areas of stress concentrations of the a) Araldite 2020 (brittle) and b) Araldite 2047-1 (ductile) adhesive joints subjected to in-plane bending loading with and without environment exposure. Numerical results for joints represent predictions by the CZM methodology.

The stiffness response of the joints was accurately predicted by the CZM approach for both adhesives. It is worth noting, however, that experimentally, during the in-plane loading test, uneven loading conditions led to non-linear strain response towards the end of the test. The uneven loading is attributed to the gradual development of damage in different parts of the joint. It was not attempted to capture the uneven loading conditions in the numerical model.

Regarding the strength capacity of the joints, for the out-of-plane bending loading, the CZM model overpredicted the failure loads by 32% and 23% for the brittle and ductile adhesive joints, respectively. For the in-plane bending loading, the CZM approach overpredicted the maximum load capacity of the brittle adhesive joints by 17% and underpredicted the load capacity of the ductile adhesive joints by 9%.

Regarding the accuracy of the predictions, it should be noted that the CZM laws were calibrated based on the results of the DCB/SLB tests. It is important to highlight however, that the degradation of the bonded joints depends on the level of moisture ingress and the percentage of the joint that is affected by moisture. The double lap shear joints and the DCB/SLB specimens have different geometry and therefore different percentages of each joint are affected. Moreover, the excess adhesive on the sides of the double lap shear joints may be more efficient in sealing the interface, as opposed to the DCB/SLB specimens that had no protection on the sides. Nonetheless, the two tests showed clear similarities such as the moisture ingress ring on the sides and the stress whitening in the central parts of the joints which justify the good agreement between the experimental data and the CZM predictions. It can be argued that damage development is controlled mostly by the diffusion of the moisture and less by the degradation of the bulk material properties.

Further to the discussion of the failure loads, it should be noted that the numerical analyses suggest that the environmental exposure also affected the joint behaviour for the two adhesives differently with respect to the loading at the onset of damage. The load at damage onset reduced drastically for the brittle adhesive for all load cases, while it remained almost unchanged for the ductile adhesive as shown in Figures 14-17. This can be explained by the input data for the two adhesives before and after environmental degradation. The damage initiation is controlled by the initiation stress in fracture modes I and II (see Tables 5-6). Thus, for the brittle adhesive the initiation stress drops significantly for both fracture modes I and II (50-60%), while for the ductile adhesive the change is much smaller (0-20%).

4. Conclusions

The effects of environmental exposure on glass/steel adhesive joints were studied by developing a combined experimental and numerical study. The conditions examined were based on European guidelines for sealants and the degradation of the adhesive bulk properties, the interfaces and large double lap shear joint strength for the selected environmental conditions. Tensile dogbone specimens were used for the measurement of the bulk properties, and modified DCB/SLB specimens were developed and characterised for the measurement of the interface properties. For validation of the numerical methodology, large double lap shear joints were tested subjected to four different load cases; tension, compression, out-of-plane bending and in-plane bending.

The main conclusions are summarised as follows:

- With regards to the bulk properties, both adhesive systems were affected by the environmental exposure in a similar manner. The stiffness and strength reduced, while the bulk material ductility increased. The relative changes for the ductile adhesive were more significant.

- With regards to the interface properties, the trend was reversed, and the brittle adhesive exhibited larger strength reductions during the DCB/SLB tests. This shows that the interface degradation is mostly related to the moisture diffusion coefficients and the bond strength of the two adhesives to the substrate and less to the degradation of the bulk properties of the adhesives. Analysing and predicting the moisture diffusion process was considered outside the scope of this study.
- Significant strength reductions were observed for the double lap joints for all load cases. Numerical predictions of the load at damage onset revealed that the brittle adhesive experienced significant reduction in damage onset load, while this remained almost unaffected by the environmental ageing for the ductile adhesive.
- With regards to the numerical predictive methodology, the CZM approach displayed good agreement regarding the stiffness response and the failure prediction of the joints for both adhesives. The level of agreement, however, between the experimental and numerical data was reduced compared to the unaged joints due to the larger experimental scatter observed for the environmentally aged joints.
- Regarding the CM modelling methodology, this approach was accurate in predicting the stiffness response and failure behaviour of the ductile adhesive joints, when the damage was controlled by the degradation of the bulk adhesive properties. This methodology was unable however to predict the brittle adhesive joint degradation when the damage moved to the interface.
- The CZM approach is more robust and suitable since it can capture both the degradation of the bulk properties and the interfaces. A CM approach fails to account for the interface damage and can therefore only be expected to provide accurate predictions when the damage is cohesive. It is noted that this observation is based on the two adhesives investigated in this research, and conclusions may differ for other types of adhesives. For other types of adhesives, the experimental methodology outlined in this paper should be followed to determine the respective contributions of bulk and interface degradation.

Acknowledgements

The principal author gratefully acknowledges the funding from the Agency of Science, Technology and Research (A*STAR), Singapore, and the University of Southampton, United Kingdom, that has enabled the conduction of the research reported.

References

[1] Weller B., Härth K., Tasche S., Unnewehr S., Glass in Building-Principles, Applications, Examples, Birkhäuser, 2009.

[2] Haldimann M., Luible A., Overend M., Structural use of glass, International Association for Bridge and Structural Engineering, Zürich, Switzerland, 2008.

[3] IStructE, Structural use of glass in buildings, Second edition. ed., Institution of Structural Engineers, SETO, London, 2014.

[4] Van Lancker B., Dispersyn J., De Corte W., Belis J., Durability of adhesive glass-metal connections for structural applications, Engineering Structures, 126 (2016) 237-51.

[5] Machalicka K., Eliasova M., Adhesive joints in glass structures: effects of various materials in the connection, thickness of the adhesive layer, and ageing, Int J Adhes Adhes, 72 (2017) 10-22.

[6] European Organisation for Technical Approvals, ETAG 002 Guideline for European Technical Approval for Structural Sealant Glazing Kits (SSGK), European Organisation for Technical Approvals, Brussels, Belgium, 2012.

[7] Machalická K., Vokáč M., Eliášová M., Influence of artificial aging on structural adhesive connections for façade applications, Int J Adhes Adhes, 83 (2018) 168-77.

[8] Machalicka K., Vokac M., Kostelecka M., Eliasova M., Structural behavior of double-lap shear adhesive joints with metal substrates under humid conditions, International Journal of Mechanics and Materials in Design, 15 (2019) 61-76.

[9] Brewis D.M., Comyn J., Shalash R.J.A., The effect of moisture and temperature on the properties of an epoxide-polyamide adhesive in relation to its performance in single lap joints, Int J Adhes Adhes, 2 (1982) 215-22.

[10] Costa M., Viana G., Silva L.F.M.d., Campilho R.D.S.G., Effect of Humidity on The Fatigue Behaviour of Adhesively Bonded Aluminium Joints, Latin American Journal of Solids and Structures, 14 (2017) 174-87.

[11] Viana G., Costa M., Banea M.D., Silva L.F.M.d., Water Diffusion in Double Cantilever Beam Adhesive Joints, Latin American Journal of Solids and Structures, 14 (2017) 188-201.

[12] Sugiman S., Crocombe A.D., Aschroft I.A., Experimental and numerical investigation of the static response of environmentally aged adhesively bonded joints, Int J Adhes Adhes, 40 (2013) 224-37.

[13] Liljedahl C.D.M., Crocombe A.D., Wahab M.A., Ashcroft I.A., Modelling the Environmental Degradation of the Interface in Adhesively Bonded Joints using a Cohesive Zone Approach, The Journal of Adhesion, 82 (2006) 1061-89.

[14] Katsivalis I., Thomsen O.T., Feih S., Achintha M., Failure prediction and optimal selection of adhesives for glass/steel adhesive joints, Engineering Structures, 201 (2019) 109646.

[15] Katsivalis I., Thomsen O.T., Feih S., Achintha M., Development of cohesive zone models for the prediction of damage and failure of glass/steel adhesive joints, Int J Adhes Adhes, 97 (2020) 102479.

[16] British Standards Institution, BS EN 572-2:2012 Glass in building. Basic soda-lime silicate glass products. Definitions and general physical and mechanical properties Part 2: Float Glass, British Standards Institution, London, 2012.

[17] British Standards Institution, BS EN 12150-1:2015+A1:2019 Glass in building. Thermally toughened soda lime silicate safety glass. Definition and description, British Standards Institution, London, 2015.

[18] ISO, ISO 527-1:2012, Plastics – Determination of tensile properties, Part 1: General principles, International Organization for Standardization, 2012.

[19] ISO, ISO 527-2:2012, Plastics – Determination of tensile properties, Part 2: Test conditions for moulding and extrusion plastics, International Organization for Standardization, 2012.

[20] Dassault Systèmes Simulia, ABAQUS 6.14, Providence, RI, USA., 2014.

[21] Mubashar A., Ashcroft I.A., Critchlow G.W., Crocombe A.D., Moisture absorption–desorption effects in adhesive joints, Int J Adhes Adhes, 29 (2009) 751-60.

[22] da Silva L.F.M., Campilho R.D.S.G., Advances in Numerical Modelling of Adhesive Joints, Springer-Verlag Berlin Heidelberg, Berlin, 2012.

[23] Campilho R.D.S.G., Banea M.D., Neto J.A.B.P., da Silva L.F.M., Modelling adhesive joints with cohesive zone models: effect of the cohesive law shape of the adhesive layer, Int J Adhes Adhes, 44 (2013) 48-56.

[24] Sorensen B.F., Cohesive law and notch sensitivity of adhesive joints, Acta Mater., 50 (2002) 1053-61.

[25] Carlberger T., Stigh U., Influence of Layer Thickness on Cohesive Properties of an Epoxy-Based Adhesive—An Experimental Study, The Journal of Adhesion, 86 (2010) 816-35.